Agent-Directed Tracing of Multi-Scale Drug Disposition Events within Normal and Diseased In Silico Livers

Sean H. J. Kim, University of California, San Francisco, USA

Sunwoo Park, University of California, San Francisco, USA

Glen E. P. Ropella, Tempus Dictum, Inc., USA

C. Anthony Hunt, University of California, San Francisco, USA

ABSTRACT

Cirrhosis, a chronic liver disease, alters hepatic drug disposition; however, little is known about micro-mechanisms underpinning disease progression and how they contribute to changes in liver disposition properties. In this article, the authors present multilevel, agent-based and agent-directed In Silico Livers (ISLs) to probe plausible micro-mechanistic details for a cationic drug, diltiazem, in two different types of cirrhotic rat livers. Starting with ISLs that validated against diltiazem disposition data from normal livers, the authors systematically transformed ISL characteristics to achieve validation against perfusion outflow profiles from the two types of diseased livers. In this regard, the authors developed and implemented multilevel methods to trace each object representing diltiazem during simulated perfusion experiments. This enabled gaining heretofore-unavailable insight into plausible micro-mechanistic details from diltiazem's perspective in normal and diseased livers. The authors posit that the presented ISL micro-mechanistic details may have disease caused counterparts during disposition.

Keywords: Cirrhosis, Drug Disposition, In Silico Liver, Multi-Scale Tracing, Simulation Experiment

INTRODUCTION

Cirrhosis includes chronic, advanced fibrosis (scarring) of liver, a major site of drug metabolism and clearance. It results from the perpetuation of the normal wound healing response and subsequent distortion of hepatic histoarchitecture. The disease complicates drug therapy management because it alters hepatic drug disposition, which, in turn, alters pharmacokinetic (PK) and/or pharmacodynamic characteristics. The nature of that alteration is dependent on the nature and the extent of disease. With some exceptions (Hung et al.,

DOI: 10.4018/jats.2010070101

2002), little is known about exactly how the cirrhotic changes affect hepatic drug disposition. Improved, mechanistic insight is needed to enable rational drug therapy based on clinical measures of both type and extent of liver disease.

We have used a new strategy to achieve improved insight. It involves developing and experimenting on multi-scale In Silico Livers (ISLs) (Park, Ropella, Kim, Roberts, & Hunt, 2009). Key ISL and support components were represented as independent, interacting agents. In silico experiments were conducted using an automated, high-performance software environment capable of parallel computation. We started with ISLs that validated for drug and sucrose disposition profiles of normal rat livers in situ (Yan, Ropella, Park, Roberts, & Hunt, 2008). The models were then subjected to cycles of experimentation and iterative refinement to achieve simulated drug disposition profiles that were acceptably similar to those from two different types of diseased livers (Hung et al., 2002). The diseased ISLs were created independently: for each type, an increasing number of normal ISL characteristics were altered systematically until simulated drug disposition profiles were experimentally indistinguishable from the referent profiles.

Having achieved a degree of validation, we posit that the causative, mechanistic details occurring during ISL execution may have hepatic counterparts during disposition, as diagrammed in Figure 1. Differences in micro-mechanistic details between the normal and the two "diseased" ISLs are hypotheses about corresponding differences between the normal and diseased livers, and about differences between diseased livers. Achieving a degree of profile similarity is evidence supporting those hypotheses. The differences in dynamic, multilevel details during execution of the two diseased ISLs provide a plausible, physiologically based explanation of the disease-caused differences in hepatic drug disposition. With additional rounds of refinement and validation, future ISLs are expected to provide increasingly useful scientific predictions and deeper insight into mechanistic details of disease progression and its role in hepatic PK.

BIOLOGY

Liver and Cirrhosis

Liver is the largest glandular organ (~1.5 kg; human), which plays a central role in drug metabolism and clearance (Arias et al., 2009). Cells composing the liver are organized into roughly hexagonal units called lobules. Hepatocytes occupy the majority of lobular volume. Each lobule is organized around a central vein that drains blood into the hepatic vein. Along its periphery, a lobule is associated with hepatic portal vein and artery networks that deliver incoming blood. Vessels, lined by endothelial cells, branch among the hepatocytes, forming sinusoids into which the blood flows.

Cirrhosis distorts hepatic tissue architecture and vasculature (Schiff, Sorrell, & Maddrey, 2003). Loss of endothelial fenestrations and filling of the space of Disse, a permeable connective tissue interface between endothelia and hepatocytes, can be observed as disease progresses. Various factors such as chronic alcoholism and hepatitis contribute to cirrhotic development. Major clinical consequences include impaired hepatocyte (liver) function, alterations in drug disposition, and circulatory abnormalities. Currently available therapeutic treatments primarily focus on reducing complications and preventing further degeneration.

In Situ Liver Perfusion

The original single-pass perfusion experiments are summarized in Figure 2; full details are provided in (Hung et al., 2002). Normal livers and two types of cirrhotic liver were studied. Both diseased types followed a similar pretreatment protocol to induce cirrhotic changes: one was produced by chronic carbon tetrachloride (CCl_4) treatment; the other was by chronic alcohol (ethanol) treatment. Both treatments induced hepatic injury, but their histologies were different. Chronic CCl_4 treatment produced acute hepatocellular injury with centrilobular necrosis and stenosis, whereas alcohol treatment resulted in hepatocellular injury with inflam-

Figure 1. Relationships between perfused rat liver models and In Silico Livers (ISLs). (A) Perfused rat livers in their experimental context are the referent systems. During experiments, liver components interact with transiting drug molecules causing changes in the compound's outflow profile. Systemic behaviors at all levels are reflected in the collected data. (B) ISL components are designed, coded, verified, and assembled based on mechanism and component descriptions that are physiologically based. Concretizable mapping 1 is intended to exist from ISL components and interactions to hepatic physiological and micro-anatomic details. System dynamics during execution (mapping 2) are intended to abstractly represent plausible corresponding dynamics occurring within the liver during disposition. Measures of dynamics provide time series data that are intended to mimic counterpart measures of wet-laboratory perfusion experiments. Achieving measurable similarities makes mapping 3 quantitative. (C) Diseased counterparts to normal ISLs can be achieved by iteratively altering a subset of normal parameter values, mechanisms, and events into diseased counterparts that validate. Conceptual mappings are offered to relate differences in parameter values (normal to diseased) to measures of histopathology.

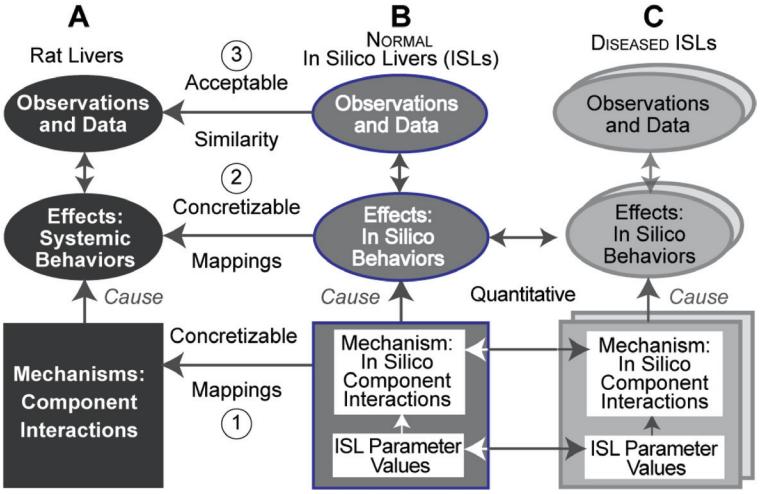

mation and perivenular degeneration. Control, normal PK profiles were obtained using livers from matched rats treated identically, absent either CCl_4 or alcohol treatment. Nine outflow profiles of diltiazem were analyzed individually using established PK methods.

MODEL

Relational Grounding

The units, dimensions, and/or objects to which a variable or model component refers establish groundings. Inductive PK models are typically grounded to metric spaces. So doing provides simple, interpretive mappings between output and parameter values and referent data. However, metric grounding creates issues that must be addressed each time one needs to expand the model to include additional phenomena and when combining models to form a larger system. Adding a term to an equation, for example, requires defining its variables and premises to be quantitatively commensurate with everything else in the model. Such expansions can be challenging and even infeasible when knowledge is limited and uncertainty is high, which is the situation that we faced. The reusability of such a metrically grounded model is limited under different experimental conditions or when an assumption made is brought into question.

Figure 2. In situ liver perfusion. Details of the original experiments are provided in (Hung et al., 2002). Briefly, the carbon tetrachloride (CCl_4) rat model was established by feeding male Wistar rats with CCl_4 given by intragastric gavage for 12 weeks. The alcohol rat model was developed by feeding a high-fat liquid alcohol diet containing ethanol. Both diets induced fibrosis. After 12 weeks, the animals were subjected to laparotomy and cannulization of the portal vein and bile duct. Non-circulating perfusions were made via the portal vein cannula. Bolus dose containing a target drug (e.g., diltiazem) was injected into the liver with outflow samples collected by a fraction collector. After perfusion, the animals were killed by thoracotomy.

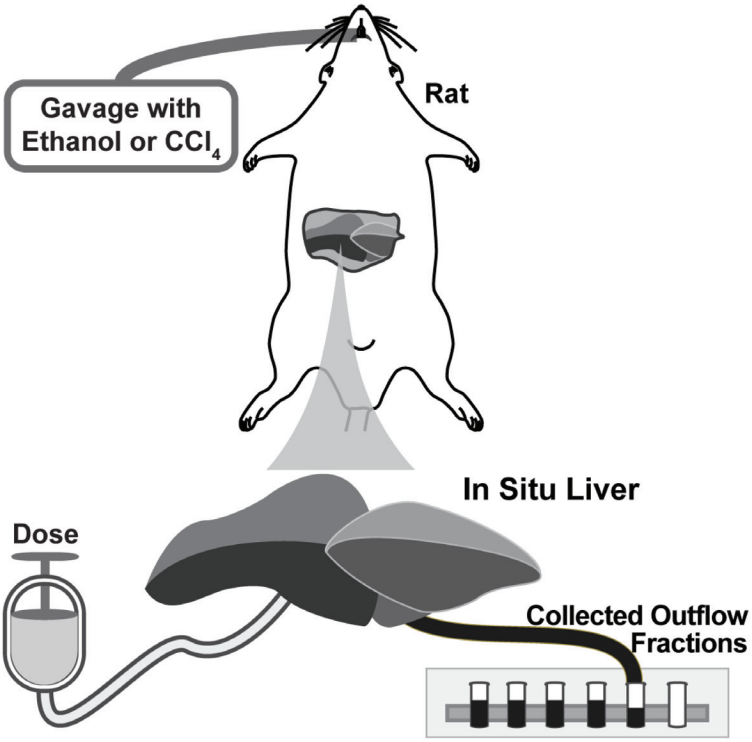

In order to develop and begin validating concretized drug disposition theories for normal and diseased states, we need the ability to simultaneously explore different regions of plausible mechanism space at different levels of detail, and relate results to wet-laboratory observations. To facilitate that process it must be easy to change mechanistic details at any level without having to invest significant time in ISL reengineering. The solution is to remove metric grounding from the ISL and confine it to quantitative feature-to-feature and phenomena-to-phenomena mapping models. Each ISL component is grounded to other components rather than to a metric imposed by an outside observer: they are relationally grounded. So doing enables synthesizing flexible, easily adaptable ISL components that meet our requirements.

In Silico Liver

Detailed descriptions of ISL design and the mappings between ISL components and mechanisms and liver histology and physiology are available in (Hunt, Ropella, Yan, Hung, & Roberts, 2006; Park et al., 2009; Yan et al., 2008). To clearly distinguish in silico components and processes from corresponding hepatic structures and

processes, hereafter we use small caps when referring to the ISL counterparts.

An ISL simulation framework corresponds to an entire wet-laboratory experimental system. It comprises an experiment agent, which is a highly abstract analogue of the scientists conducting liver perfusion experiments, a data management module, a statistical observer module, a parameter manager, and three different models: *DatModel*, *RefModel*, and *ArtModel*. *DatModel* is the referent data from (Hung et al., 2002). *RefModel* is a classical, two-phase stochastic PK model fitted to *DatModel* (Hung et al., 2002). The fitted model predicts the time course of diltiazem in liver effluent during a perfusion experiment.

ArtModel is the complete system illustrated in Figure 3. As in (Hunt et al., 2006), we assumed that anatomical and physiological characteristics of all hepatic lobules, normal and diseased, are somewhat similar. Each ISL is thus a collection of similar LOBULES. However, a collection of heterogeneous LOBULES can be easily implemented, should that be required. To represent a single outflow profile, we pool results from executions of 48 Monte Carlo variants of a single, parameterized LOBULE; those pooled, averaged results comprise one ISL PERFUSION experiment.

Lobular Components

The relative arrangement of hepatic function and flow is represented at the LOBULE level using a directed graph called sinusoid network. Each Monte Carlo variant of a network maps to a distinct arrangement of flow paths from portal vein tracts (PV) to the lobular central vein (CV). A sinusoid network is subdivided into three zones. The number of nodes per zone is always Zone I > Zone II > Zone III. Zone I, being close to PV, always has more nodes; Zone III, being next to CV, has the fewest. Zonation enables mimicking quantitative and functional differences between periportal and perivenous lobular regions (Gaudio, Onori, Franchitto, Sferra, & Riggio, 1997). A graph edge specifies a flow connection between two nodes. Lobular variability within and between livers is simulated by having edges assigned pseudo-randomly at the start of each of the 48 LOBULAR runs.

A Sinusoidal Segment (SS) is an agent that represents all needed aspects of sinusoid function. One SS is assigned to each graph node. Each SS is somewhat different and the stochastic differences are parameter controlled. SS counts per zone were Zone I = 45, Zone II = 20, and Zone III = 5. As explained in (Hunt et al., 2006), these numbers were needed for sufficient PV-to-CV path variety to reduce fluctuations within outflow profiles. The SSs were connected using a minimum of 109 edges: 39 intra-Zone I edges, 8 intra-Zone II connections, 37 Zone I-to-Zone II, and 25 Zone II-to-Zone III connections. All Zone III nodes were connected to CV. Two SS types were used: direct (larger, shorter; controlled by the *DirSin* parameters) and tortuous (thinner, longer; controlled by the *TortSin* parameters).

A SS consists of a Core and three layered toroidal spaces, as illustrated in Figure 3. The Core maps to blood flow. It provides a direct PV-to-CV path. Spaces A–C have the same dimensions. Space A maps to the interface between vascular blood flow and the endothelial layer. Space B is called the ENDOTHELIAL layer. It maps to easily accessible spaces and cells presumed to be primarily endothelial cells. Space C is called the HEPATOCYTE layer. It maps to less accessible spaces and cells, primarily the space of Disse, hepatocytes, and bile canaliculi. CELLS in Space B are called ENDOTHELIAL CELLS; those in Space C are called HEPATOCYTES. Parameters allow the resolution of the spaces to be increased (or decreased) as needed.

CELLS contain objects that are needed to represent required intracellular processes such as drug binding, metabolism, transport, and sequestration. It is known that basic compounds such as diltiazem are sequestered in organelles such as lysosomes and mitochondria, as well as being bound (Hung et al., 2002; Siebert, Hung, Chang, & Roberts, 2004). However, motivated by parsimony, sequestration and binding were not resolved: everything within a cell that

Figure 3. Hierarchical, multilevel structure of an In Silico Liver (ISL). A LOBULE *maps to the functional unit of the liver, which consists of portal vein tracts (PV), a central vein (CV), and interconnected sinusoids. Blood flows from PV to CV. A* LOBULE *network is specified using an interconnected directed graph having Sinusoidal Segment (SS) nodes organized into three zones. Intra-zonal connections are possible. Inter-zone connections link SS nodes from Zone 1 to 2, from 1 to 3, and from 2 to 3. A SS maps to a unit of sinusoid structure and function. It contains a Core and three two-dimensional toroidal grid spaces. Space A maps to the interface between blood flow and cells. Space B is the* ENDOTHELIAL *layer, which comprises* ENDOTHELIAL CELLS *and spaces in-between. Space C is called the* HEPATOCYTE *layer; it contains* HEPATOCYTES *and* EXTRACELLULAR *spaces.* ENDOTHELIAL CELLS *and* HEPATOCYTES *contain* BINDERS *that can bind* COMPOUNDS. BINDERS *in* HEPATOCYTES *function as* METABOLIZING ENZYMES. *Objects representing* DRUG *move within and between spaces;* DRUG *can move in and out of* CELLS.

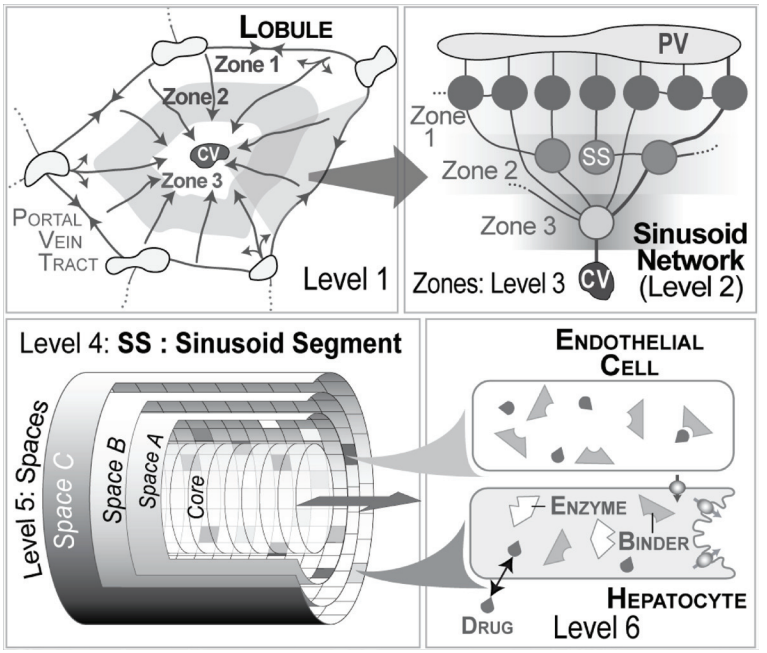

can bind or sequester diltiazem is conflated and represented by some number of identical binding objects (hereafter, simply BINDERS). BINDERS inside HEPATOCYTES are called ENZYMES. An ENZYME BINDING event can end with release of METABOLITE.

ISL Parameters

ISL parameters specify structural and functional properties, experiment configuration, and dosage characteristics. We used the same set of parameters detailed in (Park et al., 2009).

One ISL simulation experiment averages 48 Monte Carlo executions of one LOBULE. The duration of each execution is specified by *cycleLimit*. The number of steps executed each cycle is *stepsPerCycle*. The execution-cycle-step hierarchy enabled observing and analyzing ISL experiments using two time resolutions. DRUG disposition is observed at cycle resolution; spatiotemporal activities are traced at step resolution. One simulation cycle maps to 0.5 seconds, the finest resolution of the validation data. *CycleLimit* and *stepsPerCycle* were set to 200 and 2, respectively.

The following parameters govern structural and spatiotemporal SS properties and components at lower ISL levels. *DirSinRatio* and *TortSinRatio* specify the ratio of the two SS types. SS circumference and length are generated using the values of *DirSinCircMin*, *DirSinCircMax*, *TortSinCircMin*, *TortSinCircMax*, *DirSinLenAlpha*, *DirSinLenBeta*, *DirSinLenShift*, *TortSinLenAlpha*, *TortSinLenBeta*, and *TortSinLenShift*. COMPOUND movements from one SS space to another are governed by *A2BJumpProb*, *B2AJumpProb*, *B2CJumpProb*, and *C2BJumpProb*. Simulated blood flow (in the Core) and local, biased random walk (Spaces A-C) are controlled by *CoreFlowRate* and *SinusoidTurbo*; their values can depend on the COMPOUND'S physicochemical properties. *ECDensity* and *HepDensity* specify the number of ENDOTHELIAL CELLS and HEPATOCYTES in Spaces B and C, respectively. The number of BINDERS in a CELL is Monte Carlo determined and is within the range specified by *BindersPerCellMin* and *BindersPerCellMax*. *SoluteBindingProb* specifies the probability of BINDING for a COMPOUND located within a BINDER'S local neighborhood. *SoluteBindingCycle* sets the duration of each BINDING event. The latter two parameters also depend on the COMPOUND'S physicochemical properties.

A set of parameters defines COMPOUND properties and characteristics. *MetabolizeProb* is the probability that a METABOLITE, rather than its parent COMPOUND, will be released from an ENZYME-COMPOUND complex. *ISLWetLabScaling* is a scaling factor used to map COMPOUNDS exiting CV directly to perfusate concentration in situ. *MembraneCrossing* is a binary property of each COMPOUND, which specifies whether that particular COMPOUND can enter CELLS.

Compound Disposition

We describe ISL disposition functions from the perspective of a COMPOUND traversing through a LOBULE. At the start of simulation, a parameter specified number of COMPOUNDS is instantiated and placed in PV. Initially these COMPOUNDS move into connected SSs through the Core and Space A. Their movements are biased random walks toward CV. At any time, a COMPOUND can move (jump) from Space A to B, or from B to C, or vice versa with a parameter specified probability (*A2BJumpProb*, *B2AJumpProb*, *B2CJumpProb*, or *C2BJumpProb*). A COMPOUND positioned next to a HEPATOCYTE or ENDOTHELIAL CELL can be taken into the CELL. A CELL contains some number of BINDERS, one of which binds the TRANSPORTED COMPOUND with a parameter specified probability (*SoluteBindingProb*). BINDERS inside HEPATOCYTES can METABOLIZE the COMPOUND and release a METABOLITE. For all other BINDING events, the COMPOUND is released after parameter specified duration (*SoluteBindingCycle*). The released COMPOUND continues its travel through linked SSs and between SS spaces until it reaches CV, at which point the COMPOUND is collected and removed from the system.

Similarity Measure

ISL outflow profiles were compared with referent profiles using the quantitative Similarity Measure (SM) defined previously (Hunt et al., 2006; Park et al., 2009; Yan et al., 2008). An ISL outflow profile was accepted as valid—as being indistinguishable experimentally from an in situ profile—when SM > 0.9. The SM measures the fraction of collected COMPOUNDS that lies within a band that was a prespecified, scaled factor of referent outflow values:

$$SM_1(p_s, p_r, s, e, k) = \frac{\sum_{i=s}^{e} C(p_r^l(i,k) \le p_r^u(i,k))}{(e-s+1)} \quad (1)$$

where p_s: simulated hepatic disposition outflow profile; p_r: in situ hepatic disposition outflow profile; $s,e \in \boldsymbol{Z}^+$: start and end simulation cycle number; μ: sample mean of p_r ; $\gamma_r = (p_r - \mu)/\mu$; $k \in \boldsymbol{R}^+$: scaling factor of the $\pm k \cdot \sigma(\gamma_r)$ band; $p_r^l(i,k) = p(i)(1 - k \cdot \sigma(\gamma_r))$: lower bound of the band; $p_r^u(i,k) = p(i)(1 + k \cdot \sigma(\gamma_r))$: upper bound of the band; $\sigma(\gamma_r)$: standard deviation of γ_r; $C(cond) = 1$ if the *cond* is true, otherwise 0; and $k =$

0.5, 0.75, or 1.0. Both raw and smoothed ISL profiles were scored.

Multi-Scale Event Tracing

Tracing disposition events within and between ISL levels was divided into two phases. In the first phase, all spatiotemporal events involving COMPOUNDS (of the same type) and their interactions with components across levels were recorded. A trace data file was generated for each SS including PV and CV, which tracked the temporal order of events involving COMPOUNDS that resided within that SS. To trace METABOLIC events, each SS also generated a tracing file that listed the COMPOUND'S ID along with the TIME METABOLISM occurred.

In the second phase, collected raw data were reorganized and translated into analytical tracing measures for evaluation. We started by tracing changes at Levels 1 and 2 (Figure 3): changes associated with ENDOTHELIAL CELLS, HEPATOCYTES, ENZYMES, and BINDERS at Level 1 and within the four SS spaces. Tracing results at higher levels were deduced by aggregating results from lower levels. Tracing measures included the path traversed by each COMPOUND, a COMPOUND'S resident TIME within ISL features, and the fraction of BOUND or UNBOUND COMPOUNDS in each SS. Those measures were used to assess how micromechanisms differed between NORMAL and DISEASED ISLs.

ISL Execution

ISL experiments followed execution steps diagrammed in Figure 4. The process was designed to provide improved lifecycle management, execution efficiency, tracing quality, and analysis of traced results. It has eight steps. In Step 1, an ISL experiment is configured with a specification file that describes the structural topology of a LOBULE, an ISL parameter file that lists all parameters and their values, and a parameter-sweeping file that specifies a non-linear discrete region of ISL parameter space to be swept. A parameter sweeping space corresponds to a collection of parameter name-value files, which are dynamically constructed from the ISL parameter and sweeping files by a parameter sweeper. In Step 2, the sweeping space is decomposed into a set of partition blocks in the group level parallel mode, which is a coarse-grain parallelism (described below). In Step 3, a set of multiple Monte Carlo runs of a single parameter file is decomposed into a set of partition blocks in the experiment level parallel mode, which is a fine-grain parallelism (described below). In Step 4, partition blocks are dispatched to a set of computation nodes. In Step 5, simulation at each computation node runs concurrently using a parameter file or a collection of Monte Carlo runs depending on the parallel mode. In Step 6, local analysis is conducted simultaneously at each computation node, followed by a posteriori analysis on local analytic results. These two-phase analyses improve overall performance. All analytical results are stored within a shared file system. Step 7 applies if parameter sweeping is activated, and the experiment continues until all parameter sets in the sweeping space are completed. Otherwise, Step 8 applies to end the experiment.

Parallel executions were performed in different modes to improve performance compared to monotonic parallelism or sequential execution. Each parallel mode was associated with one of the six ISL levels or an experimental requirement. Heterogeneity in parallel execution helped achieve improved performance along with efficient resource management. ISL parallel mode, as illustrated in Figure 4, was supported at group and experiment levels. Group level parallel mode enabled executing multiple experiments in parallel by segregating each experiment and allowing each to run concurrently without interaction. Parallel batch processing and analysis of local execution results were performed using that mode. Experiment level parallel mode enabled executing single experiments in parallel as separate LOBULE Monte Carlo variants. Top-level system components including simulation coordinator, parallel batch processor, parallel model partitioner and deployer managed the overall parallel execution process.

Figure 4. ISL execution process. ISL experiments are enabled for parallel execution managed by top-level system components including parallel batch processor, partitioner, and deployer. At the start of an experiment, a set of parameter space files are dynamically constructed from ISL parameter and sweeping files and LOBULE specifications. Next, based on the parameter space files and parallel execution mode selected, the experiment is decomposed into a set of partition blocks and dispatched for execution to a set of computation nodes. Simulation data are analyzed simultaneously at each node, followed by a posteriori analysis on local results. If parameter sweeping is activated, the experiment continues until all parameter sets in the sweeping space are completed. Otherwise, the experiment ends, and open files are closed.

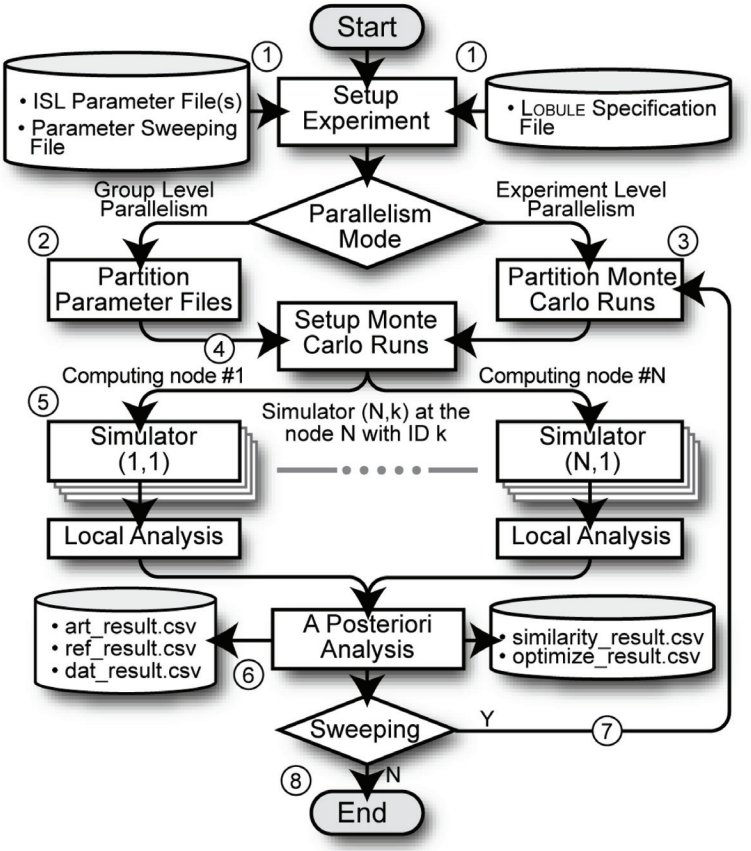

Implementation Tools

System framework was implemented using Swarm 2.2 (www.swarm.org) on a small-scale Beowulf cluster consisting of one master node and seven client nodes. We used MPICH (www-unix.mcs.anl.gov/mpi/mpich1/) for parallelization. Simulation and tracing results were analyzed using R 2.7.1 (www.r-project.org) and MATLAB (www.mathworks.com).

MODEL VALIDATION

Starting with validated NORMAL ISLs (Park et al., 2009; Yan et al., 2008) and the diltiazem outflow profiles from a CCl_4-treated liver as referents, we iteratively adjusted NORMAL ISL parameter values to change the properties of DILTIAZEM outflow profiles. We continued that adjustment process until the outflow profile achieved SM

> 0.9. The resulting, validated ISL was called DISEASED$_{CCl4}$ ISL. We then repeated that protocol with the diltiazem outflow profiles from an alcohol-treated liver as the referent. ISL that achieved validation was called DISEASED$_{ALC}$ ISL.

The following is an illustration of iteratively adjusting parameters of the validated NORMAL ISL toward those of DISEASED$_{ALC}$ ISL. We first needed to adjust the probabilistic movements of COMPOUNDS in DISEASED$_{ALC}$ so that the outflow fraction near the peak (< 15 SECONDS) was close to that of a NORMAL outflow profile, but lower after 15 SECONDS. To achieve the first, we tuned *A2BJumpProb* and *B2AJumpProb* to values smaller than those of the validated NORMAL ISLs. When using the same dosing function, the shape and height of an outflow profile around its peak was very sensitive to changes in those two parameters. We also tuned *BinderPerCell* for DISEASED$_{ALC}$ to be smaller than those of NORMAL ISLs. That adjustment also contributed to the placement of the outflow profile's peak because it determined the population densities of BINDERS and ENZYMES in Spaces B and C. To achieve a lower outflow fraction after the peak, we increased *B2CJumpProb* but lowered *C2BJumpProb* relative to the values of NORMAL ISL. Consequently, more COMPOUNDS entered Space C in DISEASED$_{ALC}$ ISL, but they were delayed in reaching CV. An increase in METABOLIC events in Space C was also an important factor contributing to a lowered outflow profile. Similar adjustments were made to other parameters to incrementally improve outflow similarity until the ISL achieved SM > 0.9.

Table 1 lists parameter values that were changed to achieve validation for DISEASED$_{CCl4}$ and DISEASED$_{ALC}$ ISLs. Note whereas twelve LOBULAR parameter adjustments were needed to validate DISEASED$_{CCl4}$ ISL, only six were needed to validate DISEASED$_{ALC}$ ISL. Except for the *C2BJumpProb* adjustments, the magnitude of the adjustments needed for DISEASED$_{ALC}$ ISL was smaller than those of DISEASED$_{CCl4}$ ISL. Overall, the parameter value changes are consistent with less profound and fewer observed pathological changes caused by alcohol pretreatment (Hung et al., 2002).

DILTIAZEM outflow profiles from each of the three ISLs are graphed in Figure 5. SM values for unsmoothed profiles were 0.92 (NORMAL), 0.92 (DISEASED$_{CCl4}$), and 0.91 (DISEASED$_{ALC}$). SM values for smoothed data are listed in Figure 5. Hereafter, unless stated otherwise, all results are reported in the order NORMAL, DISEASED$_{CCl4}$ and, DISEASED$_{ALC}$, when values for all three are provided, and DISEASED$_{CCl4}$ and DISEASED$_{ALC}$ when only DISEASED ISL values are provided.

Previous studies have detailed how the generative consequences of ISL parameters are networked and nonlinear (Park et al., 2009; Yan et al., 2008). A small change in one parameter can be offset by adjustments of other parameters. Consequently, studies of sensitivity to individual parameters are less informative and less meaningful than are location changes in ISL parameter space. Individually, the parameter changes in Table 1 did not cause statistically significant changes in outflow profiles. In general, a 5% change in any one parameter would not result in a visible change in outflow profiles. However, a 5% change in all parameters can cause a significant change. The changes in Table 1 averaged 32% for DISEASED$_{CCl4}$ ISLs and 18% for DISEASED$_{ALC}$ ISLs.

TRACING DILTIAZEM DISPOSITION

From raw DILTIAZEM tracing data, any number of derived measures can be obtained, and each enables viewing disposition from a different perspective. Each provides a somewhat different image of events occurring within ISLs during simulations. Some measures may be useful in helping us think about ISLs (e.g., what change may be needed during parameter tuning to move closer to targeted phenomena). Others may be helpful in thinking about hepatic disposition of the referent compound. Still others may be helpful in thinking about different disease consequences and even disease progression. Here we focus our analysis on DILTIAZEM movements within LOBULES, which highlight functional and

Table 1. Parameter differences between NORMAL and DISEASED ISLs

Parameter	Normal	$Diseased_{CCl4}$	$Diseased_{ALC}$
A2BJumpProb	0.38	0.2	0.35
B2AJumpProb	0.37	0.3	0.35
B2CJumpProb	0.55	0.34	0.65
C2BJumpProb	0.48	0.55	0.25
ECDensity	0.65	0.60	0.65
HepDensity	0.70	0.65	0.70
SoluteBindProb	0.5	0.38	0.50
BinderPerCell	95	65	75
SoluteBindCycles	11	28	10
SSTypeRatio	19	99	19
DirSinCirc	24	22	24
SinusoidTurbo	0.82	0.85	0.82

structural differences between NORMAL and DISEASED ISLs.

Figure 6 shows how stochastic DILTIAZEM movements within the three spaces influenced average DILTIAZEM resident TIMES. The bar graphs (Figure 6A-C) specify the DOSE fraction having resident TIMES within the indicated ten-SECOND range. For both DISEASED ISLs, there was a reduction in DILTIAZEM having 0–10 SECOND resident TIMES, and an increase in DILTIAZEM having 10–20 SECOND resident TIMES. The net effect for both DISEASED ISLs was an increase in DILTIAZEM having longer resident TIMES, which is evident in the bar graphs. The two DISEASE types altered resident TIME patterns differently (Figure 6B,C). Surprisingly, there were no significant differences in mean (and SD) DILTIAZEM resident TIMES: 47.8 (26.0), 48.8 (25.2), and 45.9 (26.5) SECONDS. Several factors influenced the differences between resident TIMES. *A2BJumpProb* differences between the three ISL types (0.38, 0.21, and 0.35) caused fewer DILTIAZEM to move into Space B in DISEASED relative to NORMAL LOBULES. Similarly, differences in *B2CJumpProb* (0.55, 0.34, and 0.65) caused fewer of the DILTIAZEM that did reach Space B in $DISEASED_{CCl4}$ relative to $DISEASED_{ALC}$ to move into Space C.

The path length data shown in Figure 6D-F are measures of the cumulative length of all SSs entered by each DILTIAZEM. All three ISL types had 70 SSs distributed among the three zones. On average, NORMAL and $DISEASED_{ALC}$ ISLs had 3.5 of the long, narrow SSs, whereas only occasionally did a $DISEASED_{CCl4}$ ISL have even one. Consequently, a small subset of DILTIAZEM path lengths in NORMAL and $DISEASED_{ALC}$ ISLs were long, but they were essentially absent in the $DISEASED_{CCl4}$ ISLs. The SSs in Zone 1 map to the interconnections between sinusoids that are most numerous in the periportal region but are absent in the perivenous region of normal lobules. Microscopy evidence suggests that some of those interconnections are lost in CCl_4-treated, cirrhotic lobules (Gaudio et al., 1997).

We recorded each DILTIAZEM'S SINUSOID traverse path for 100 SECONDS after dosing: until it exited the LOBULE, was METABOLIZED, or the run ended. Path lengths were divided into two types: complete and incomplete. In the above order, the mean percent of the dose that ended at CV was 47, 59, and 38%, whereas 23, 9, and 29% ended at a SS (and was METABOLIZED). Passage was still in progress when the run ended for 30, 32, and 33% of the DILTIAZEM dose. The average

Figure 5. Outflow profiles of DILTIAZEM *in* NORMAL *and* DISEASED *ISLs. Smoothed* DILTIAZEM *outflow values are plotted for (A)* NORMAL*, (B)* $DISEASED_{ALC}$*, and (C)* $DISEASED_{CCl4}$ *ISLs. They achieved validation by having Similarity Measure (SM) > 0.9. The SM computes the fraction of collected* COMPOUNDS *that lies within a band (± 33%) around the referent outflow values. ISL data shown are averages of 48 Monte Carlo runs. Solid lines connecting referent outflow data are graphed along with the output of the fitted mathematical model (dotted curves) (Hung et al., 2002).*

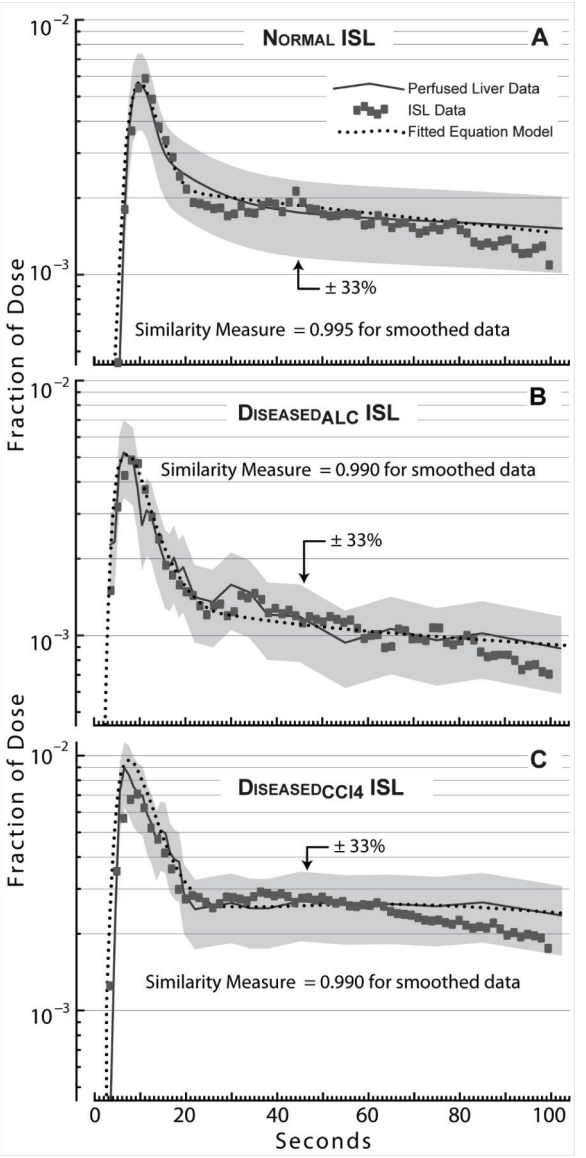

path lengths, in the above order, were 64, 59, and 55 (in grid units). The shorter mean paths for DISEASED ISLs show that both types of DISEASE made it easier for DILTIAZEM to move closer to CV as TIME advanced. It is evident from Figure 6D-F that $DISEASED_{CCl4}$ ISLs had a more narrowly

distributed variety of path lengths. Note also that the DISEASED$_{CCl4}$ ISLs had significantly fewer of the shortest paths (0–25 grid units) than either NORMAL or DISEASED$_{ALC}$ ISLs.

An informative perspective is provided by observing DILTIAZEMS percolate through individual SSs in different LOBULAR zones. Selected results are graphed in Figure 7 for similarly sized SS in each of the three zones, which show the fraction of DILTIAZEM DOSE within Core and Spaces A–C of the selected SS. Differences in relative trends between the three zones are striking. Zone 2 peaks occur later than those in Zone 1. The amount of DILTIAZEM trickling through Zone 3 was still increasing at 40 SECONDS for all three ISLs. The relative patterns for NORMAL and DISEASED$_{ALC}$ SSs within the same zone were similar and clearly different from those in the DISEASED$_{CCl4}$ SSs. Notably, the DISEASED$_{CCl4}$ SSs exhibited a dramatic increase in the binding of DILTIAZEM within the ENDOTHELIAL layer, thus preventing movement into the HEPATOCYTE layer. That may map to the observed fibrotic changes retarding diltiazem's access to spaces more distant from blood flow.

For the tracing results, one DILTIAZEM within one SS grid site can be viewed as mapping to a wet-laboratory lower limit of detection. For example, it may be viewed as the limit of detection of referent compound in a biopsy sample that has a volume 1/5000th that of an average lobule. At that limit, some biopsy samples will test negative for compound, even though we are confident some is present. By analogy, an empty grid site within the ISL during simulation cycle maps to "no detectable drug." Even though we can trace the change in location of a specific DILTIAZEM during execu-

Figure 6. DILTIAZEM resident TIMES and traversal path lengths in NORMAL and DISEASED ISLs. (A-C) Resident TIME measures the amount of TIME a DILTIAZEM resides in a LOBULE. Each DILTIAZEM was traced from initial injection until it was METABOLIZED, cleared from the LOBULE through the CENTRAL VEIN (CV), or the simulation run ended. Shown are average resident TIME histograms for (A) NORMAL, (B) DISEASED$_{ALC}$, and (C) DISEASED$_{CCl4}$LOBULES. Bar heights measure the fraction of dose having resident TIMES within the indicated ten-SECOND interval. (D-F) Path length measures the total length (in grid units) of Sinusoidal Segments visited by a DILTIAZEM. Shown are average path length histograms for (D) NORMAL, (E) DISEASED$_{ALC}$, and (F) DISEASED$_{CCl4}$LOBULES. Histogram bin size is 25 grid units. Bar height corresponds to fraction of administered DILTIAZEMS.

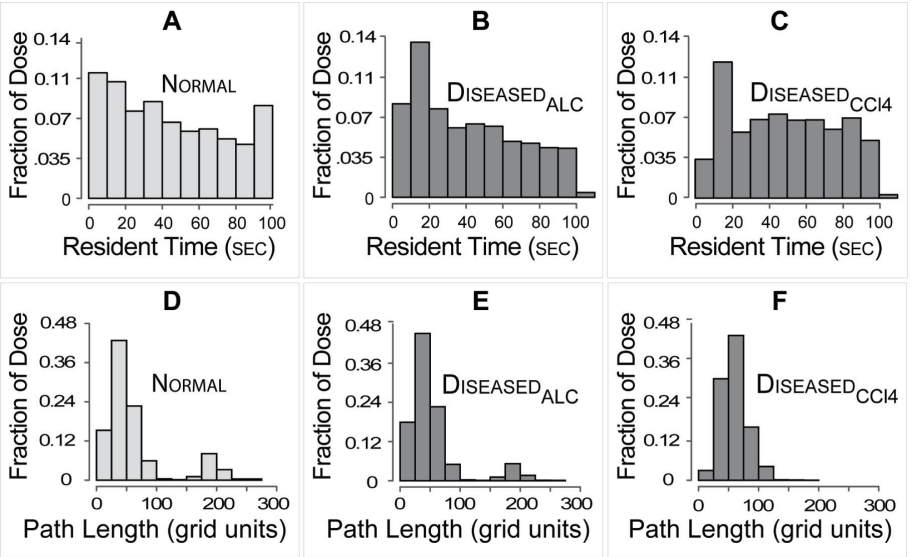

Figure 7. Fraction of DILTIZEM *dose that was* BOUND *or* UNBOUND *within different sinusoidal segment (SS) spaces in each zone. Similarly sized segments were selected from Zone 1 (three left panels), Zone 2 (three center panels), and Zone 3 (three right panels) from a* NORMAL *(three top panels), a* $DISEASED_{ALC}$ *(three middle panels), and a* $DISEASED_{CCl4}$ *ISL (three bottom panels). In each panel, the* DOSE *fraction (regardless of location or state) that is* BOUND *or* UNBOUND *in* HEPATOCYTES *(in Space C) or in* ENDOTHELIAL CELLS *(in Space B) at indicated times is plotted. The curves are approximate trend lines.*

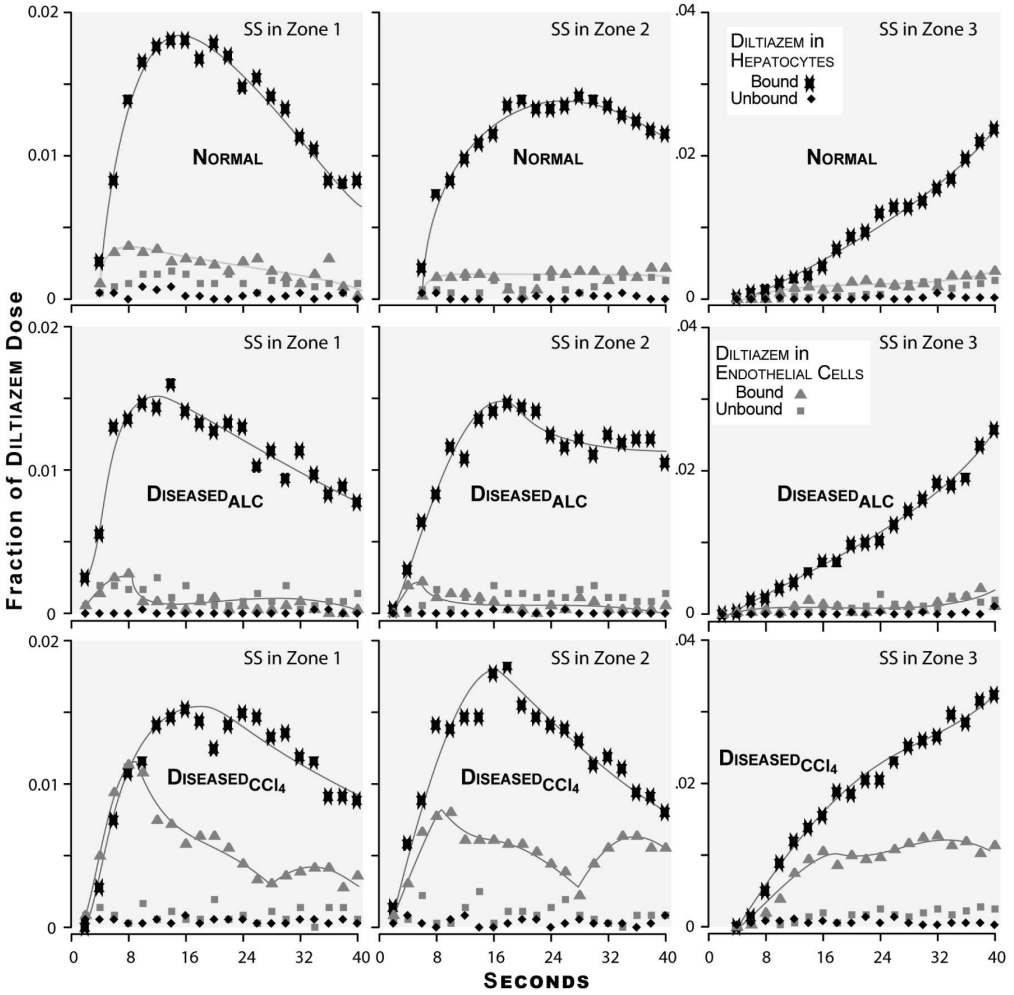

tion, there is no mapping to corresponding changes in location for specific molecules. A DILTIAZEM object maps to some number of actual molecules. From one simulation cycle to the next, that number of molecules is unchanged. However, the actual molecules to which a DILTIAZEM object maps may not be the same from one simulation cycle to another.

RELATING ISL DIFFERENCES TO MEASURES OF DISEASE

Wet-laboratory data on disposition-related features are coarse-grained, whole liver measures taken at the end of the experiment, whereas ISL parameters influence fine-grained, spatio-temporal events occurring during simulation.

Consequently, the two sets of data are not easily compared. Nevertheless, to the extent that the mappings shown in Figure 1 are reasonable, we can conjecture how DISEASED ISL properties might map to pathologic changes occurring within cirrhotic liver. For example, permeability, called the permeability-surface product by Hung et al. (2002), is a derived measure of water's ability to permeate lobular tissue. *A2BJumpProb* maps well to this measure. The pattern of change in *A2BJumpProb* also may map to number of fenestra, which counts fenestrae in comparable tissue sections. Fenestrae influence the ability of all material, especially larger material, to exit blood and access the space of Disse (Wisse et al., 1996). In ISL Space B, an ENDOTHELIAL CELL is the lower limit of spatial resolution. Fenestrae are below that level of resolution and thus have no ISL counterpart. However, grid spaces not assigned to ENDOTHELIAL CELLS map to extracellular spaces, and so a subset may map to fenestrae.

Collagenization, which is increased in different ways in the two disease models, would be expected to make it harder for a compound to move into tissue spaces, and harder to return once there. In the DISEASED ISLs, DILTIAZEM movement between spaces governed by *JumpProb* parameters and *SinusoidTurbo* (for $\text{DISEASED}_{\text{CCl4}}$ ISL) are altered. Their complex interactions influenced resident TIMES and path lengths shown in Figure 6. One could speculate similar changes that accompany collagenization of the space of Disse and subsequently reduced exchange between sinusoids and hepatocytes. For albumin space estimation, the measure decreased for both diseased livers (Hung et al., 2002). It is a measure of the lobular volume accessible to albumin. We might expect LOBULAR resident TIMES to map somewhat to accessible space: if the spaces are smaller, then resident time should decrease, and it did. We see in Figure 6A-C that the DILTIAZEM dose fractions having longer resident TIMES decreased in both DISEASED ISLs.

CONCLUSION

For the level of abstraction used, the ISL outflow results support the idea that both mechanism and event level mappings in Figure 1 may be reasonable; i.e., they may have rat model counterparts. The incremental parameter changes that were necessary (and sufficient) to transform a NORMAL liver into a DISEASED ISL may correspond abstractly to molecular, cellular, and sinusoid level transformations responsible for the pathogenesis from normal into diseased livers during CCl_4 and alcohol treatment. The general consistency between DISEASED ISLs during execution and the cited histopathology evidence supports the hypothesis. We thus have a tentative, yet promising, in silico model that enables us to visualize, abstractly from the perspective of diltiazem, how the consequences of cirrhosis may have progressed. That new capability represents an important step toward unraveling the complex influences of disease on drug disposition.

Being able to transform one validated model into another is important. Having independently validated NORMAL and DISEASED ISLs allows one to explore plausible drug disposition consequences of intermediate levels of disease and even disease that is more advanced. Because of individual differences in disease progression, conducting wet-laboratory experiments to document the former would be problematic, and the latter may be deemed unethical. By assuming disease progression corresponds to gradual change from NORMAL to DISEASED ISL parameter values, we can simulate a liver that has progressed half way, for example, along the path to the currently documented disease state. We can project further parameter changes to explore plausible consequences of more advanced level of disease. Corresponding explorations of intermediate and advanced disease states would be infeasible using traditional inductive mathematical models. Ultimately, the approach can facilitate rational translation of research

results to useful applications, and that may open doors to development of strategies for tailoring drug choices to help reverse disease conditions.

Making progress toward the long-term goals requires more sophisticated, detailed features. One such feature pertains to SS graphs, which, in current implementation, are abstract, randomized networks of SS nodes that have no concrete mapping to the spatial structure of sinusoids within referent liver lobules. For this study, because outflow profiles were our validation data, there was no need to make LOBULES explicitly spatial. Adding such a requirement merely for the purpose of making the structure of the LOBULE more intuitive or "more like" the referent, absent any fine-grained spatial data against which to validate, runs counter to the parsimony guideline. On the other hand, there is some reasonable pressure to make the LOBULES spatially explicit. Lobular zonation and sinusoidal structure data exist and are explicitly spatial (Gebhardt, 1992; Jungermann, 1995). Because current LOBULES can contain graphs that cannot project onto a 3D vector space, validation against such zonation data is infeasible. Doing so would be more straightforward if the ISL LOBULES were spatially explicit. We are considering making them so in future experiments.

Figure 8. The iterative refinement and validation protocol. The objective is to discover spatio-temporal mechanisms that will generate desired ISL behaviors during experiments. The initial steps involve selecting a small but diverse set of targeted hepatic attributes, static and dynamic, and specifying appropriate Similarity Measures (SMs) and their target values. Next, we posit, implement, and instantiate ISL mechanisms, requiring as few components as is reasonable, that may generate analogous phenomena. Simulation experiments are conducted to measure ISL behaviors and evaluate similarity to hepatic data. When the prespecified level of similarity is achieved, we can proceed to increase the level of SM target values or expand the attribute list until the ISL is falsified. Once the ISL is falsified, return to the earlier steps for further refinement.

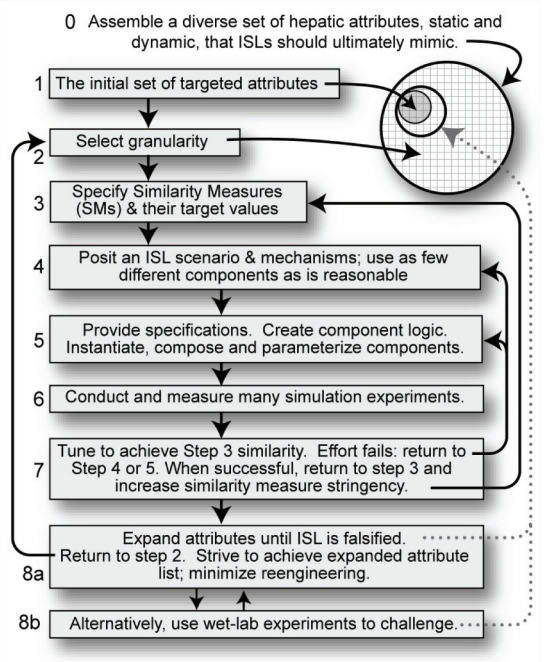

The iterative modeling and experimentation process, as illustrated in Figure 8, is an integral part of ISL development (Hunt et al., 2006; Park et al., 2009). That protocol supports adhering to the guideline of parsimony which is important when building a complex model. It also involves continual evaluation and testing of the model and implementation details, which helps build a degree of confidence in the model accuracy (i.e., verification). For this study, we started with ISLs that have been extensively tested and scrutinized to insure achievement of prespecified Similarity Measure values. Because the transformation from NORMAL to DISEASED ISLs did not involve changes to the actual implementation, model verification was not a central focus herein. Moving forward, the continual, rigorous model verification will be critical to insuring confidence as existing ISL features are modified or new details added.

ACKNOWLEDGMENT

We thank Michael Roberts at University of Queensland Australia and members of the UCSF BioSystems group for helpful suggestions and discussions. We gratefully acknowledge research funding provided by the CDH Research Foundation. This paper is extended from "Agent-Based Simulation of Drug Disposition in Cirrhotic Liver" published at *Spring Simulation Multiconference 2010, Agent-Directed Simulation Symposium,* Orlando, Florida, USA, April 12-14, 2010. We will present in a separate manuscript different aspects of the micromechanistic details recorded during these experiments.

REFERENCES

Arias, I. M., Alter, H. J., Boyer, J. L., Cohen, D. E., Fausto, N., Shafritz, D. A., & Wolkoff, A. W. (Eds.). (2009). *The liver biology and pathobiology* (5th ed.). Chichester, UK: John Wiley & Sons Ltd.

Gaudio, E., Onori, P., Franchitto, A., Sferra, R., & Riggio, O. (1997). Liver metabolic zonation and hepatic microcirculation in carbon tetrachloride-induced experimental cirrhosis. *Digestive Diseases and Sciences*, *42*, 167–177. doi:10.1023/A:1018813911469

Gebhardt, R. (1992). Metabolic zonation of the liver: regulation and implications for liver function. *Pharmacology & Therapeutics*, *53*, 275–354. doi:10.1016/0163-7258(92)90055-5

Hung, D. Y., Chang, P., Cheung, K., McWhinney, B., Masci, P. P., Weiss, M., & Roberts, M. S. (2002). Cationic drug pharmacokinetics in diseased livers determined by fibrosis index, hepatic protein content, microsomal activity, and nature of drug. *The Journal of Pharmacology and Experimental Therapeutics*, *301*, 1079–1087. doi:10.1124/jpet.301.3.1079

Hunt, C. A., Ropella, G. E. P., Yan, L., Hung, D. Y., & Roberts, M. S. (2006). Physiologically based synthetic models of hepatic disposition. *Journal of Pharmacokinetics and Pharmacodynamics*, *33*, 737–772. doi:10.1007/s10928-006-9031-3

Jungermann, K. (1995). Zonation of metabolism and gene expression in liver. *Histochemistry and Cell Biology*, *103*, 81–91. doi:10.1007/BF01454004

Park, S., Ropella, G. E., Kim, S. H. J., Roberts, M. S., & Hunt, C. A. (2009). Computational strategies unravel and trace how liver disease changes hepatic drug disposition. *The Journal of Pharmacology and Experimental Therapeutics*, *328*, 294–305. doi:10.1124/jpet.108.142497

Schiff, E. R., Sorrell, M. F., & Maddrey, E. C. (2003). *Schiff's diseases of the liver* (9th ed.). Philadelphia, PA: Lippincott, Williams & Wilkins.

Siebert, G. A., Hung, D. Y., Chang, P., & Roberts, M. S. (2004). Ion-trapping, microsomal binding, and unbound drug distribution in the hepatic retention of basic drugs. *The Journal of Pharmacology and Experimental Therapeutics*, *308*, 228–235. doi:10.1124/jpet.103.056770

Wisse, E., Braet, F., Luo, D., De Zanger, R., Jans, D., Crabbé, E., & Vermoesen, A. (1996). Structure and function of sinusoidal lining cells in the liver. *Toxicologic Pathology*, *24*, 100–111. doi:10.1177/019262339602400114

Yan, L., Ropella, G. E. P., Park, S., Roberts, M. S., & Hunt, C. A. (2008). Modeling and simulation of hepatic drug disposition using a physiologically based, multi-agent in silico liver. *Pharmaceutical Research*, *25*, 1023–1036. doi:10.1007/s11095-007-9494-y